Reply for the referee comment#2

General comments

Model predictions of chemical composition in dust aerosols and its effect on iron solubility and ocean biogeochemistry are highly uncertain. The authors implemented a mineralogical map and atmospheric processing schemes of dust to a global atmospheric chemistry model. They evaluated the model results against observations of total and soluble iron concentrations. They conducted sensitivity experiments to assess the impact of recent shifts in dust emissions and chemical compositions on soluble iron deposition in the Northwest Pacific. Their results indicate a decreasing trend in dust soluble iron deposition from East Asia to the Northwest Pacific by 2.4% per year, primarily due to reduced dust emissions, which are mainly driven by declining surface winds over dust source regions. They show an increasing trend in dust iron solubility from 1.5% in 2001 to 1.7% in 2017. This increased iron solubility is associated with the acidification of coarse mode aerosols due to the increase in anthropogenic NO_x emissions and in-cloud oxalate-ligand-promoted dissolution. The modeling exercises in this paper may help us to advance modeling dust iron. However, the differences of their model development from previous studies are unclear in its current form. It is more appropriate to cite parent papers rather than the following papers to clarify the model development. I have some comments and questions to improve this paper.

General response: We would like to express our gratitude for your detailed and insightful feedback. Below, we provide responses to each comment and indicate how the manuscript will be revised accordingly.

Specific comment#1: l.89: How did you calculate Na^+ on dust?

Response: Thank you for your insightful comment. We didn't calculate Na^+ on dust. The Na^+ in Eq.3a are mainly sourced from sea-salt aerosol and the concentration is calculated for each aerosol modes but not the specified aerosol type. In our study, the CAM-chem model employed the MOSAIC module to calculate aerosol pH for four aerosol modes: Aitken, Accumulation, Coarse, and Primary Carbon. Different types of aerosols, such as sulfate, nitrate, dust, and sea-salt, are externally mixed between the modes and internally mixed within each mode (Liu et al., 2016). The ion concentration is calculated for each mode and this includes both dust and sea-salt aerosols. Na^+ in the model primarily originates from sea-salt aerosols, which are represented by electrolytes such as Na_2SO_4, $NaNO_3$, and NaCl.

Reference

Liu, X., Ma, P. L., Wang, H., Tilmes, S., Singh, B., Easter, R. C., Ghan, S. J., and Rasch, P. J.: Description and evaluation of a new four-mode version of the Modal Aerosol Module (MAM4) within version 5.3 of the Community Atmosphere Model, Geosci. Model Dev., 9, 505-522, 10.5194/gmd-9-505-2016, 2016.

Specific comment#2: l.98 and Fig. 7: What are the criteria using either (4a) or (4b)? Please elucidate how alkaline cations as in (3a) are considered for pH calculation in the sulfate-poor conditions to understand the acidic conditions in coarse particles over the oceans (see below comments on Fig. 7).

$$m_{H^+} = 2m_{SO_4^{2-}} + m_{HSO_4^-} + m_{NO_3^-} + m_{Cl^-} - (2m_{Ca^{2+}} + m_{NH_4^+} + m_{Na^+}) \quad (3a)$$

$$m_{H^+} = \frac{K^{gl}_{HNO_3} C_{l,HNO_3}}{\kappa_{HNO_3} m_{NO_3^-} (\gamma_{HNO_3})^2}, or \quad (4a)$$

$$m_{H^+} = \frac{K^{gl}_{HCl} C_{l,HCl}}{\kappa_{HCl} m_{Cl^-} (\gamma_{HCl})^2} \quad (4b)$$

Response: The criteria for using equations (4a) and (4b) depend on the equilibrium concentrations of nitrate and chloride in both the gas and aerosol phases. Specifically, equation (4a) is applied when HNO_3 gas and NO_3 aerosol are both present and have concentrations greater than zero while Equation (4b) is used when HCl gas and chloride aerosol concentrations are greater than zero after computing equilibrium surface concentrations.

In sulfate-poor conditions, it is important to account for the gas-aerosol exchange of semi-volatile gases such as HNO_3, HCl, and NH_3. Using the internal equilibrium H+ concentration like Eq.3 would lead to oscillations in the condensation and evaporation of these gases, as it does not provide steady-state results (Zaveri et al., 2008). Therefore, MOSAIC employs dynamic H+ concentrations which is determined by equilibrium constants, mass transfer coefficients, and the gas- and particle-phase concentrations of all involved semi-volatile species like Eq.4. Alkaline cations as described in Eq.3a have no effect on the pH calculation in sulfate-poor conditions. We have specified the pH mechanism in line 102.

Line 102: "Under sulfate-poor conditions ($XT > 2$), it is important to account for the gas-aerosol exchange of semi-volatile gases such as HNO_3, HCl, and NH_3. Using the internal equilibrium H+ concentration would lead to oscillations in the condensation and evaporation of these gases, as it does not provide steady-state results (Zaveri et al., 2008). Therefore, MOSAIC employs dynamic H+ concentrations which is determined by gas-particle exchange of semi-volatile acidic gases (HNO_3 and HCl) predominantly controls aerosol acidic pH as follows (Eq.4):

…

calculated by MOSAIC (Zaveri et al., 2008; Zaveri et al., 2005a; Zaveri et al., 2005b). Specifically, equation (4a) is applied when HNO_3 gas and NO_3 aerosol are both present and have concentrations greater than zero while Equation (4b) is used when HCl gas and chloride aerosol concentrations are greater than zero after computing equilibrium surface concentrations."

Reference

Zaveri, R. A., Easter, R. C., Fast, J. D., and Peters, L. K.: Model for Simulating Aerosol Interactions and Chemistry (MOSAIC), Journal of Geophysical Research: Atmospheres, 113, https://doi.org/10.1029/2007JD008782, 2008.

Specific comment#3: l.112: This mineralogy map has been implemented by previous studies. Please cite the parent papers rather than your references and elucidate the differences from previous studies.

Response: Thank you for your insightful comment. We have specified the reference paper and added a discussion in the line 124.

Line 124: "In this study, a detailed mineralogy map database (Nickovic et al., 2012) was implemented into the CAM6-chem model to configure the mineral composition of dust emissions. This map is based on the work of Claquin et al. (1999) and has been widely used in previous modeling studies (Johnson and Meskhidze, 2013; Ito and Xu, 2014; Myriokefalitakis et al., 2015). The map segments soil into silt/clay fractions and includes five main iron minerals: hematite, smectite, illite, kaolinite, and feldspar. Notably, compared to the mineralogy map from Journet et al. (2014), this map has been shown to perform well, particularly in identifying phyllosilicates with high soluble iron content (Gonçalves Ageitos et al., 2023)."

Specific comment#4: Please specify iron content and initial iron solubility in minerals.

Response: Thanks for your insightful comment. We have added Table S2 to provide the iron content and initial iron solubility for each of the five minerals. The statement is in line 135.

Table S2. Iron content and initial iron solubility for each of the five minerals

	Fe_rs	Fe_ms	Fe_ss	Fe content	Fe solubility
Hematite	0%	0%	57.5%	57.5%	0%
Smectite	0.55%	10.45%	0%	11.0%	5%
Illite	0.11%	3.89%	0%	4.0%	2.8%
Kaolinite	0.01%	0%	0.23%	0.24%	4.2%
Feldspar	0.01%	0%	0.33%	0.34%	2.9%

Line 135: "On top of the mineralogy, …with proportions aligned with Hamilton et al. (2019) and Scanza et al. (2018). The detailed iron content and initial iron solubility for each of the five minerals have been shown in Table S2."

Specific comment#5: l.119: This scheme has been implemented by previous studies. Please cite the parent papers rather than your references and elucidate the differences from previous studies.

Response: Thanks for your insightful comment. We have now included the parent papers and expanded the discussion in line 135.

Line 135: "On top of the mineralogy, …with proportions aligned with Hamilton et al. (2019) and Scanza et al. (2018). The detailed iron content and initial iron solubility for each of the five minerals have been shown in Table S2. These values are sourced from measurements (Journet et al., 2008; Shi et al., 2011a; Shi et al., 2011b) and are consistent with previous modeling studies (Ito and Xu 2014; Scanza et al., 2018; Hamilton et al., 2019)"

Specific comment#6: l.122, Figure S1: Please show the comparison of iron content with observations to prove the underestimations of dust iron in main dust source regions by default settings and discuss the major reasons.

Response: Thanks for your insightful comment. We have added the global distribution of initial iron content in dust coarse mode aerosol as Figure S1a and discussed it in the article in line 138.

Line 138: "According to the utilization of the mineralogy map, our model achieved to simulate the global spatial patterns of total and initial soluble iron emissions. Compared to the default setting of 3.5%, the total iron content in dust aerosol is higher in the main dust sources including North Africa, Middle East and central Asia, and East Asia (Fig. S1a). This is consistent with the observations (Lafon et al., 2004, 2006; Shi et al., 2011b) and the research by Ito and Xu (2014), which reported that the observed iron content in North Africa and East Asia averaged 3.7%. Therefore, the use of the mineralogy map increases the iron content in dust from these regions (Fig. S1b) which suggest the default settings likely underestimate dust iron in these main dust source regions."

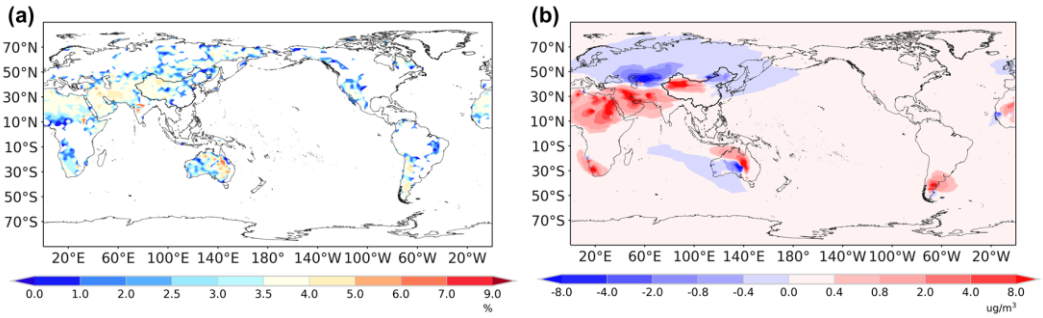

Figure S1. (a) Spatial distribution of iron content in coarse mode dust aerosol. (b) Compared to the default setting (3.5% iron in dust), changes in dust total iron surface concentrations from the developed model averaged 2001-2017 springs.

Specific comment#7: l.124: The two atmospheric processing has been implemented by previous studies. Please cite the parent papers rather than your references and elucidate the differences from previous studies.

Response: Thanks for your insightful comment. We have added the parent papers and discussed the differences from previous studies that included atmospheric processing in line 145 and line 165.

Line 145: "For proton-promoted dissolution, we employ the first-order dissolution rate formula of Lesaga et al. (1994) as follows (Eq.5) for interstitial iron aerosols:

$$RFe_{i,proton} = K_i(T) \times a(H^+)^{m_i} \times f(\nabla G_r) \times A_i \times MW_i \quad (5a)$$

$$\frac{d}{dt}\left[Fe_{sol,\ proton}\right] = RFe_{i,proton} \times [Fe_{insol}] \quad (5b)$$

…, A is the specific surface area and MW is the molecular weight. The parameters for the first-order dissolution rate formula (Eq. 5) are based on previous studies (Meskhidze et al., 2003; Ito and Feng, 2010; Ito and Xu, 2014) and are aligned with Scanza et al. (2018) and Hamilton et al. (2019). For $K_i(T)$ in Fe_ms type, here we use the dissolution rate of mineral illite as an additional simplification following Scanza et al., (2018). In contrast, some studies (Ito and Feng, 2010; Ito, 2012; Ito and Xu,

2014) employ separate dissolution rates for different minerals. For $K_i(T)$ in Fe_ss type, we use a fast dissolution rate with three stages, following Ito and Xu (2014)."

Line 165: "For oxalate-promoted dissolution, we employ the first-order dissolution rate formula for cloud-borne iron aerosols as follows (Eq.6):

$$RFe_{i,oxalate} = a_i \times [C_2O_4^{2-}] + b_i \quad (6a)$$

$$\frac{d}{dt}\left[Fe_{sol,\ oxalate}\right] = RFe_{i,oxalate} \times [Fe_{insol}] \quad (6b)$$

…, coefficients a_i and b_i are determined by Paris et al., (2011) and aligned with Scanza et al., (2018) and Hamilton et al., (2019). This linear relationship between oxalate-promoted dissolution rate and oxalate concentration in solution is based on cloud water studies by Paris et al. (2011) and has been employed in previous modeling studies (Johnson and Meskhidze, 2013; Myriokefalitakis et al., 2015). Furthermore, Ito and Shi (2016) developed a new oxalate-promoted scheme, which has been applied in recent research (Myriokefalitakis et al., 2022)."

Specific comment#8: l.135, Figure S2: Did you use the annually averaged pH values? Please rephrase observed pH, because there is no direct measurement of pH in aerosol. Since this study focuses on coarse mode aerosols, why don't you show the similar figure for the coarse mode to support the model performance?

Response: Thanks for your insightful comment. The annually averaged pH values were used in this study. We have replaced "observed" with "observationally estimated" to clarify that there are no direct measurements of pH in aerosols. The lack of sufficient observations makes it challenging to provide a detailed comparison for the model performance with respect to coarse mode aerosols. We have made revisions as follows.

Line 158: "The simulated aerosol pH in accumulation and coarse mode have been shown in Figure S2. The fine particles are relatively more acidic while coarse-mode particles are significantly less acidic influenced by sea salt and dust components. Through the annually averaged comparison of accumulation mode aerosols' pH with observations collected by Pye et al. (2020), our model successfully captured the global characteristics of fine aerosol pH. The correlation coefficient and normalized mean bias (NMB) are 0.4 and 27% respectively. The discrepancy could be attributed by the seasonal variations and the dynamics of precursor gas emissions, environmental factors such as relative humidity."

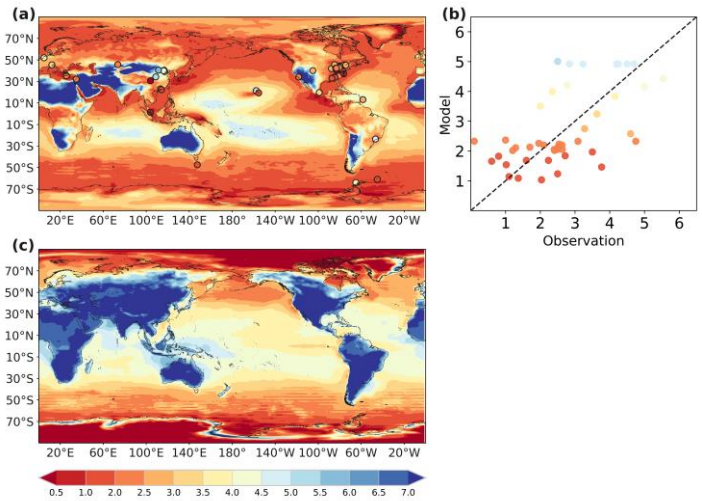

Figure S2. (a) Spatial distribution of aerosol pH in accumulation mode in 2013 and observationally estimated ground-level fine-aerosol pH (dots) from Pye et al. (2020). (b) The linear relationship between aerosol pH simulation and observationally estimated ground-level fine-aerosol pH. (c) Spatial distribution of aerosol pH in coarse mode in 2013.

Specific comment#9: l.147 and section 3.3.3: Please show the comparisons with observed oxalate levels in East Asia cloud water.

Response: We have gathered global oxalate observations in rain/cloud water to provide a more detailed comparison. The references have been listed in supplementary. Figures S4 in the supplementary material show the spatial distribution of observation locations and the evaluation of the simulation. We have expanded the oxalate comparison in line 182 as follows:

Line 181: "For the oxalate evaluation, we have collected global oxalate observations in rain/cloud water to evaluate our model results. The locations and months are consistent between observations and the model. Comparisons with observed oxalate levels indicate that our model accurately captures the quantitative characteristics of oxalate especially in East Asia (Figure S4)."

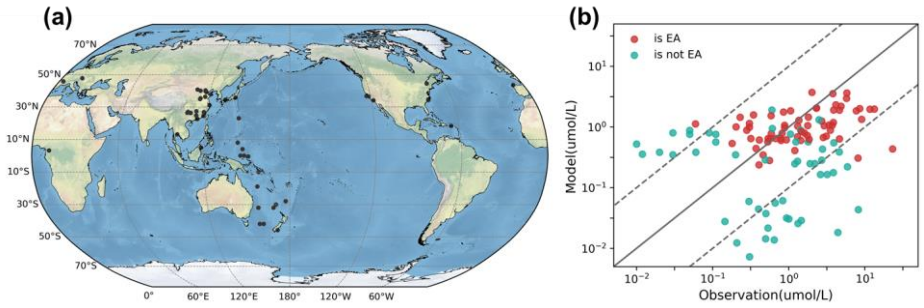

Figure S4. (a) Sample locations of the observed oxalate in rain/cloud water (Sempéré and Kawamura, 1996; Willey et al., 2000; Brooks Avery et al., 2001; Kawamura et al., 2001; Hegg et al., 2002; Kieber et al., 2002; Löflund et al., 2002; Peña et al., 2002; Kim et al., 2003; Sigha-Nkamdjou et al., 2003; Crahan et al., 2004; Hu et al., 2005; Brooks Avery et al., 2006; Xu et al., 2009; Huang et al., 2010; Huo et al., 2010; Sumari et al., 2010; Gioda et al., 2011; Wang et al., 2011; Zhang et al., 2011; Khuntong, 2012; Zhu et al., 2016; Du et al., 2017; Zhao et al., 2019;

Zhang et al., 2021; González et al., 2022; Lee et al., 2022; Xie et al., 2022; Sun et al., 2024). (b) The comparison between estimated oxalate concentration in cloud water and observations. The read circles are East Asia sites and the cyan circles are not East Asia sites.

Specific comment#10: l. 215, Figure 3: Please show the comparison of iron solubility.
Response: We have added the comparison of iron solubility as Figure S7. Our model only captures the 0-10% iron solubility range. This is likely due to the lack of pyrogenic iron which has been suggested to contribute to higher iron solubility (Ito et al., 2019). We have added a discussion in line 268.

Line 267: "What's more, the comparison about iron solubility between simulation and observations has shown in Figure S7. Our model only captures the 0-10% iron solubility. This is likely due to the lack of pyrogenic iron which has been suggested to contribute to higher iron solubility (Ito et al., 2019)."

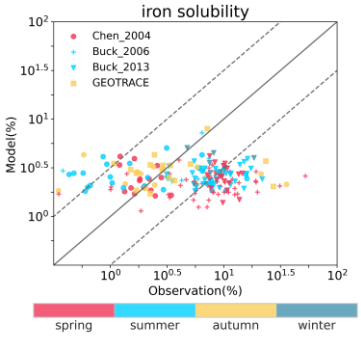

Figure S7. The comparison about iron solubility between simulation and observations.

Reference

Ito, A., Myriokefalitakis, S., Kanakidou, M., Mahowald, N. M., Scanza, R. A., Hamilton, D. S., Baker, A. R., Jickells, T., Sarin, M., Bikkina, S., Gao, Y., Shelley, R. U., Buck, C. S., Landing, W. M., Bowie, A. R., Perron, M. M. G., Guieu, C., Meskhidze, N., Johnson, M. S., Feng, Y., Kok, J. F., Nenes, A., and Duce, R. A.: Pyrogenic iron: The missing link to high iron solubility in aerosols, Science Advances, 5, eaau7671, doi:10.1126/sciadv.aau7671, 2019.

Specific comment#11: l.255: There is no reference of observational research to support this modelling results. Please correct the sentence or add the reference if any.
Response: Thanks for your insightful comment. In the study by Shi et al. (2022), observational data were used to develop a deep learning neural network (DLNN) model. Through this model, oxalate was identified as the most significant variable influencing iron solubility. We have specified the reference to this observational study in line 322.

Line 322: "And this result is consistent with previous modelling (Johnson and Meskhidze, 2013; Scanza et al., 2018) and observation research (Shi et al., 2022)."

Reference

Shi, J., Guan, Y., Gao, H., Yao, X., Wang, R., and Zhang, D.: Aerosol Iron Solubility Specification

in the Global Marine Atmosphere with Machine Learning, Environmental Science & Technology, 56, 16453-16461, 10.1021/acs.est.2c05266, 2022.

Specific comment#12: l.266, l.272 and Figure S5: It is not clear whether coarse-mode proton-promoted soluble iron deposition increased by 7% from Fig. 5. Please show the statistics for the increased trends. Please show the trend of total soluble iron deposition clearly to elucidate atmospheric processing contributed to the increase in dust iron solubility.

Response: Thanks for your insightful comment. We have added the annual trend of proton-promoted and oxalate-promoted soluble iron in fine and coarse mode as Figure S9. We expanded the discussion in line 340. We also added the linear trend in Figure S10 to show atmospheric processing contribution. We have expanded the discussion in line 340 and line 348.

Line 340: "However, the amount of soluble iron deposition produced from atmospheric processing showed a much lower decreasing rate by 18% (Figure S9). The coarse-mode proton-promoted soluble iron deposition even increased by 7% as shown in Fig. S9d."

Line 348: "We further probed into the ratios of soluble iron produced by proton-promoted and oxalate-ligand-promoted processes in total dust iron (Figure S10). The increased coarse mode proton-promoted ratio and oxalate-promoted ratio induced the increase of iron solubility (Figure S10). Our results suggested that atmospheric processing contributed to the increase in dust iron solubility..."

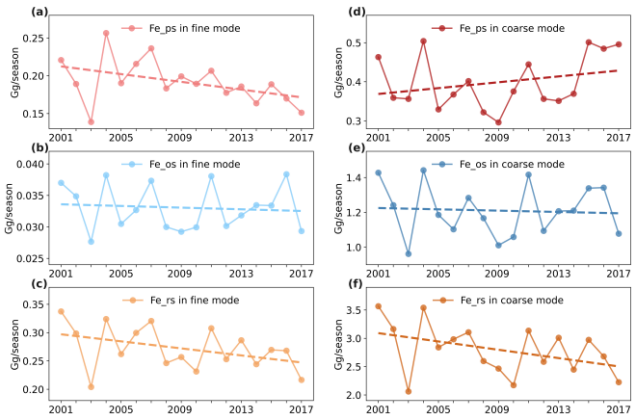

Figure S9. Temporal variations of the ratio of dust soluble iron deposition from proton-promoted (a, d), oxalate-ligand-promoted (b, e) and emissions (c, f) in coarse and fine mode (atiken + accumulation) to the Northwest Pacific averaged of 2001-2017 springs.

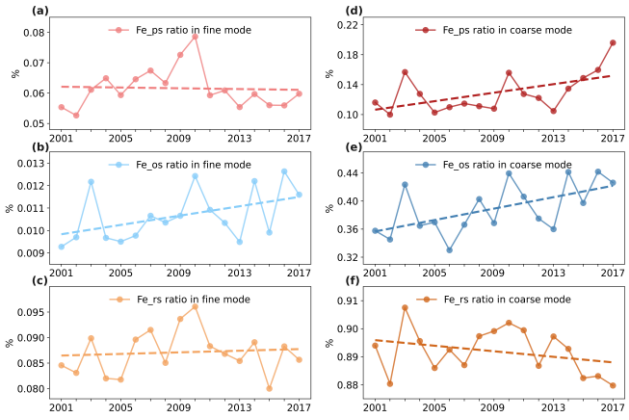

Figure S10. Temporal variations of the ratio of dust soluble iron deposition from proton-promoted (a, d), oxalate-ligand-promoted (b, e) and emissions (c, f) in coarse and fine mode (atiken + accumulation) to dust total iron deposition to the Northwest Pacific averaged of 2001-2017 springs.

Specific comment#13: l.281: The decreasing trend of dust aerosol concentration over EA and a strong correlation between surface wind speed and dust emission has been shown in previous studies, as you cited. Please discuss the similarities and differences between this and previous studies quantitatively.

Response: Thanks for your insightful comment. We have expanded the discussion in line 364.

Line 364: "This finding is consistent with previous studies (Guan et al., 2017; Wu et al., 2022; Xu et al., 2020) that also reported the dominant role of surface wind speed in the dust reduction trend in East Asia. Specifically, Guan et al. (2017) and Xu et al. (2020) focused on dust storm events and emphasized the dominant role of maximum surface wind speed based on observed datasets. Our study provided a direct relationship between dust emissions and surface wind speed. Compared to the modelling study by Wu et al. (2022) which mainly focused on the Gobi Desert, we illustrated the dust surface wind's role over the two dust sources including Gobi and Taklamakan Desert."

Specific comment#14: l.320 and Fig. 7: Since the first-order mass transfer coefficient is used to simulate size-dependent pH, HNO_3 absorption in the coarse mode should occur slowly during the long-range transport. Thus, it is unclear why pH is suddenly dropped once the aerosols are transported over the oceans. Please specify the mechanisms of quickly elevated aerosol acidity over the oceans. It is also unclear how calcite in coarse particles is consumed. Please show the spatial distribution of excess Ca (in the form of $CaCO_3$ in MOSAIC), $CaSO_4$, $Ca(NO_3)_2$ and $CaCl_2$ and specify the mechanisms of acidification of coarse particles.

Response: Thank you for your insightful comment. The first-order mass transfer coefficient is lower in the coarse mode due to the higher radius. And it would result in a slower absorption of HNO_3 during long-range transport. However, the rapid drop in pH once the coarse aerosols are transported over the oceans can be explained by several factors. Firstly, the higher relative humidity in the marine atmosphere would increase the water content of coarse mode aerosols as shown in the figure blow. This would enhance the mean wet radius ($\overline{R}_{p,m}$) of coarse mode aerosol which would enhance the first-order mass transfer coefficient ($k_{i,m}$) of HNO_3 and HCl.

$$k_{i,m} = 4\pi \overline{R}_{p,m} D_{g,i} \mathrm{N}_m f_{i,m}$$

where $k_{i,m}$ is the mass transfer rates for species i and aerosol bin m, $\overline{R}_{p,m}$ is the mean wet radius of aerosols in bin m, $D_{g,i}$ is gas diffusivity of species i, N_m is the number concentration of aerosols in bin m, and $f_{i,m}$ is the transition regime correction factor. Hence, the enhanced transfer of acidic gases induced the increased acidity of coarse mode aerosol. Secondly, pH in MOSAIC is calculated for each aerosol mode and the coarse mode is significantly influenced by sea-salt aerosols. The increased presence of sea-salt aerosols in the coarse mode over the oceans would also promote the acidification of aerosols. Thus, the combination of higher humidity and sea-salt aerosol concentration leads to a rapid drop in pH when coarse mode aerosols reach oceanic regions.

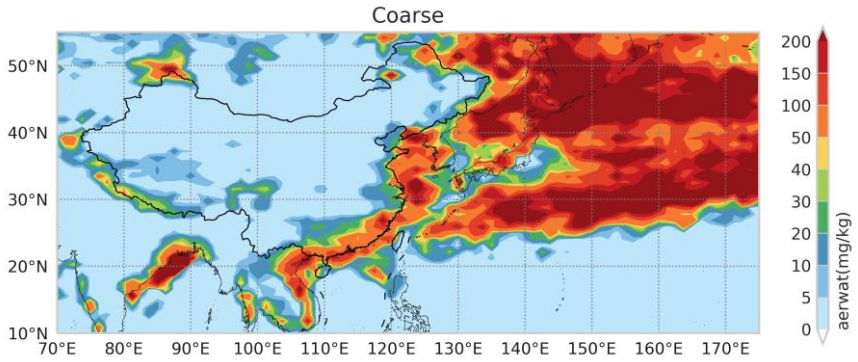

Figure. Spatial distribution of aerosol water content in coarse mode averaged of 2001 spring.

And the calcite in the particle is consumed by the following irreversible heterogeneous reactions (R1, R4, and R5) shown in Table S1. And the spatial distribution of solid-phase $CaCO_3$, solid-phase $CaSO_4$, liquid-phase $Ca(NO_3)_2$, and liquid-phase $CaCl_2$ averaged of 2001 spring has been shown in Figure S12. As dust was transported, the coarse mode solid $CaCO_3$ was consumed by HNO_3(g), H_2SO_4(g), and HCl(g) which produced $CaSO_4$, $Ca(NO_3)_2$, and $CaCl_2$ respectively. Specially, the $CaCO_3$ was mainly consumed by HNO_3(g) which produced Ca(NO3)2 due to the much higher HNO_3 gas than H_2SO_4 gas. And the maximum of $CaSO_4$ in the coastal region ([35-40N, 120-140E]) could be attributed to the R2-3 in Table S1.

We have specified the pH mechanism in line 87.

Line 87: "Firstly, the MOSAIC mechanism would determine whether the aerosol contains solid $CaCO_3$ which can adsorb acidic gases (H_2SO_4, HNO_3, and HCl). The irreversible heterogeneous reactions which would consume solid $CaCO_3$ have been listed in Table S1."

We have also further explained the acidification of coarse particles over East Asia in line 328.

Line 407: "As for coarse mode pH, it was mostly weakly alkaline according to Eq.1 (pH > 7 when T < 25℃) during spring over land areas in EA (Fig. 7b) due to the sufficient solid $CaCO_3$ content during spring over land areas in EA (Fig. S12a). The simulated quasi-neutral pH of continental coarse mode aerosols has been confirmed by thermodynamic models using aerosol samples, as reported by Fang et al. (2017) and Ding et al. (2019). During the transportation, the solid $CaCO_3$ would be consumed by acidic gases (H_2SO_4, HNO_3, and HCl) which would produce $CaSO_4$, $Ca(NO_3)_2$ and $CaCl_2$ (Figure S12). And the coarse mode aerosol pH coarse mode aerosol pH became more acidic in the coastal and ocean areas."

Table S1. List of irreversible heterogeneous reactions about Ca. (Zaveri et al., 2008)

	Irreversible heterogeneous reactions
R1	$CaCO_3(s) + H_2SO_4(g) \rightarrow CaSO_4(s) + H_2O(g) + CO_2(g)$
R2	$CaCl2(s,l) + H_2SO_4(g) \rightarrow CaSO_4(s) + 2HNO_3(g)$
R3	$Ca(NO_3)_2(s,l) + + H_2SO_4(g) \rightarrow CaSO_4(s) + 2HCl(g)$
R4	$CaCO_3(s) + 2HNO_3(g) \rightarrow Ca(NO_3)_2(s) + H_2O(g) + CO_2(g)$
R5	$CaCl2(s,l) + 2HNO_3(g) \rightarrow Ca(NO_3)_2(g) + 2HCl(g)$
R6	$CaCO_3(s) + 2HCl(g) \rightarrow CaCl_2(s) + H_2O(g) + CO_2(g)$

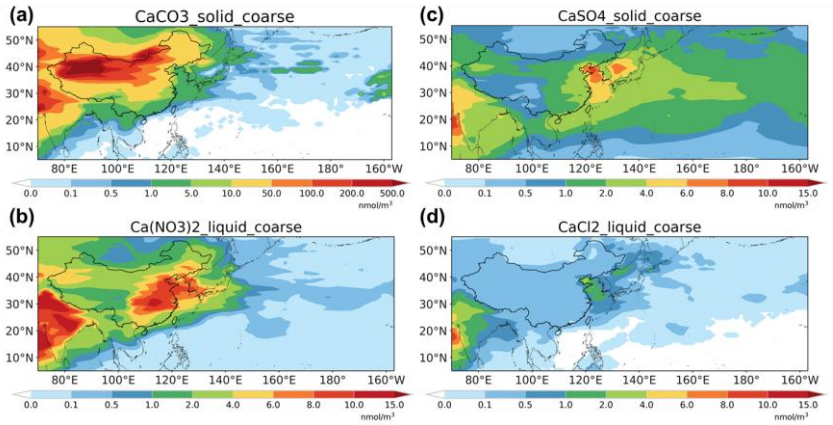

Figure S12. Spatial distributions of coarse mode solid-phase $CaCO_3$(a), solid-phase $CaSO_4$(b), liquid-phase $Ca(NO_3)_2$, and liquid-phase $CaCl_2$ averaged of 2001 spring.

Specific comment#15: l.334: Please compare with the dust aerosols, instead of sea spray aerosols cited in this sentence.

Response: Thanks for your insightful comment. We have changed to the reference about the dust aerosol acidity in line 413.

Line 413: "And coarse mode aerosol pH became more acidic in the coastal and ocean areas. The acidic pH of oceanic coarse mode aerosols which ranged from 2-5 agreed with the estimated results from mineral dust particles (Meskhidze et al., 2003)."

Reference

Meskhidze, N., Chameides, W. L., Nenes, A., and Chen, G.: Iron mobilization in mineral dust: Can anthropogenic SO_2 emissions affect ocean productivity?, Geophysical Research Letters, 30, https://doi.org/10.1029/2003GL018035, 2003.

Specific comment#16: l.341, l.445: Please explain why HCl emissions and concentrations were increased?

Response: The gas HCl in the model is not from primary emissions but secondary source. In MOSAIC, the HCl gas are from irreversible heterogeneous reactions between more acidic gases (such as HNO_3) and salt of chloride (NaCl and $CaCl_2$). It is the increased NO_x emissions induced

higher HNO_3 gas and then more HCl are product. The increased HNO_3 gas has been shown in Figure S13. We have expanded the discussion in line 424 and corrected the earlier term of HCl emissions in line 458.

Line 424: "And the increasing trend in HCl concentration was induced by the enhanced HNO_3 gas which would produce HCl gases through heterogeneous reactions with $NaCl/CaCl_2$. The increased trend has also been observed along the coast of East Asia (Gromov et al., 2016)."

Line 458: "On the one hand, the increase in iron solubility can be attributed to enhanced NO_x/HCl concentrations and reduced dust emissions"

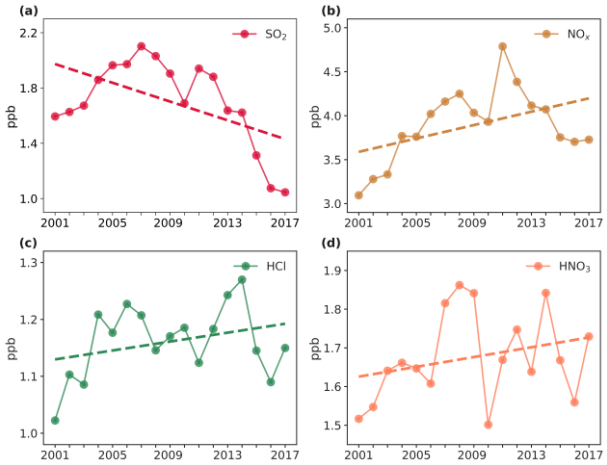

Figure S13. Temporal variations of surface concentrations of SO_2 (a), NO_x (a), HCl (c), and HNO_3(d) over the high production rate of proton-promoted soluble iron area (30-45N, 120-150E) averaged of 2001-2017 springs.

Specific comment#17: l.370: The dominant role of NO_x in the long-term trend of dust iron solubility has been shown in previous studies, as you cited. Please discuss the similarities and differences between this and previous studies quantitatively.

Response: Thanks for your insightful comment. In the study of Ito and Xu (2014), the impact of future changes in anthropogenic emissions of NO_x and SO_2 on dust soluble iron deposition to the subarctic North Pacific (40–60°N, 140–230°E) was explored. The reduction of NO_x emissions in 2100 based on the RCP4.5 compared to 2000 would lead to 15% decrease in dust soluble iron deposition promoted by acid mobilization. The changes of SO_2 emissions had negligible effect on dust soluble iron deposition. In this study, the impact of historical changes of NO_x and SO_2 emissions in 2007 spring compared to 2001 spring on dust soluble iron deposition to the Northwest Pacific (30-50°N, 140–200°E) was explored. The increased NO_x and SO_2 emissions induced 4% and 1% increased proton-promoted dust soluble iron deposition. We all have clarified the dominated role of NO_x other than SO_2 on dust soluble iron deposition. In addition, our model also indicated that changes in SO_2 emissions would also contribute to dust soluble iron deposition changes (approximately one-third of the impact of NO_x) but their model showed that SO_2 had a negligible effect. We have discussed it in line 451.

Line 451: "Our findings underscored the significant impact of anthropogenic NO_x over SO_2 on dust

soluble iron deposition historically. This result is consistent with the study by Ito and Xu (2014) which showed that future (in 2100) reductions in NO_x which were based on the RCP4.5 would lead to a decrease in soluble iron deposition over North Pacific (40–60° N, 140–230° E). However, our model also indicated that changes in SO_2 emissions would also contribute to dust soluble iron deposition changes (approximately one-third of the impact of NO_x) their model showed that SO_2 had a negligible effect."

Specific comment#18: l.386: The oxalate-promoted dissolution of iron in acidic solution is much faster than cloud water conditions according to laboratory experiments. However, the oxalate-promoted dissolution of iron in aerosol is not considered in this study. Please specify the most rapid conditions.

Response: Thanks for your insightful comment. We deleted the 'most' description and specified the occurring environment in line 466.

Line 466: "The oxalate-promoted processing takes place only when iron aerosols are in the cloud-borne phase in our model. It has been observed the enhanced iron dissolution when complexation with aerosols occurs in aqueous solutions under moderately acidic conditions such as clouds environment (Cornell and Schindler, 1987; Paris et al., 2011; Xu and Gao, 2008). This setting is consistent with the previous studies (Scanza et al., 2018; Hamilton et al, 2019) and based on the experiment study of Paris et al. (2011)."

Technical comments:

(1) l.85: Please indicate the unit of T.

Response: Thanks for your insightful comment. We have indicated it line 90.
Line 90: "The process was influenced by temperature (T) of which the unit is K as follows (Eq.1):"

(2) l.90: Please indicate the unit of m.

Response: Thanks for your insightful comment. We have indicated it line 95.
Line 95: "where m is the concentration of ions in aerosol water and the unit is mol/kg"

(3) l.95: Please indicate the unit of K. Please explain the activity coefficient used in (3b).

Response: Thanks for your insightful comment. We have indicated it in line 101.
Line 101: "where K_{HSO4} is the equilibrium constant of the bisulfate ion dissociation and the unit is $mol^2\ kg^{-2}\ atm^{-1}$ and γ is the activity coefficient of electrolyte calculated by MOSAIC"

(4) l.100: Please indicate the unit of C.

Response: Thanks for your insightful comment. We have indicated it line 110.
Line 110: "C_l is the equilibrium concentrations of acidic matter for the liquid phase and the unit is mol/m^{-3} (air)"

(5) l.173, Figure S4, and Figure 3: Please specify GEOTRACES, cite the parent papers, and follow the Fair Use Agreement (Fair_Data_Use_Statement-for-IDP2021v2.pdf).

Response: Thanks for your insightful comment. We have specified it.

Line 258: "GEOTRACES Intermediate Data Product Group (2021)"
Line 579: "We thank for the observations data from GEOTRACES. The GEOTRACES 2021 Intermediate Data Product version 2 (IDP2021v2) represents an international collaboration and is endorsed by the Scientific Committee on Oceanic Research (SCOR). The many researchers and funding agencies responsible for the collection of data and quality control are thanked for their contributions to the IDP2021v2"
Line 643: "GEOTRACES Intermediate Data Product Group (2021). The GEOTRACES Intermediate Data Product 2021 version 2 (IDP2021v2). NERC EDS British Oceanographic Data Centre NOC. doi: 10.5285/ff46f034-f47c-05f9-e053-6c86abc0dc7e"

Line 46 in supplementary: "GEOTRACES Intermediate Data Product Group (2021)"
Line 120 in supplementary: "GEOTRACES Intermediate Data Product Group (2021). The GEOTRACES Intermediate Data Product 2021 version 2 (IDP2021v2). NERC EDS British Oceanographic Data Centre NOC. doi: 10.5285/ff46f034-f47c-05f9-e053-6c86abc0dc7e"

(6) l.432: Please correct to Fig. 10 (c).

Response: Thanks for your insightful comment. We have corrected it line 511.
Line 511: "The probability distribution function of chlorophyll-a relative changes after HDEs and LDEs events over the NWP region is used to further illustrate the influence of dust iron deposition, as shown in Fig. 10(c)."